International Journal of Civil and Structural Engineering– IJCSE
Volume 2 : Issue 2 *[ISSN : 2372-3971]*
Publication Date: 19 October, 2015

Stay cables vibrations due to rain-wind interaction: a sensitivity study

Gabriele Bertagnoli Dario La Mazza Prof Giuseppe Mancini

***Abstract*—A significant correlation was observed between the occurrence of stay-cable vibrations and the combined presence of wind and rain, as the latter led to the adoption of the term Rain-Wind Induced Vibrations. This phenomenon may generate oscillations over the stays, and then over the deck, with remarkable amplitude.**
The behaviour of a large number of stays was analysed, without external damping systems, different in length, slope, diameter, tension applied and inherent damping. These cables have been exposed to different environmental conditions represented by the rain and winds agents with different wind angles and speeds.
The calibration of the used code has shown that a value of the inherent damping higher than the one actually evaluated should be used in order to obtain the vibration levels measured in reality.
The analysis of the simulations showed that the number of stays that are affected by the vibrations is small if compared to the total number of tested configurations. This is due to the fact that in order to trigger the phenomenon a number of conditions concerning the geometrical configuration, the stress state of the element, and the environmental conditions to which the structure is exposed has to occur at the same time.

Keywords-Rain-wind induced vibrations; RWIV; stay cables; bridges

I. Introduction

Nowadays stay cables are used as main structural elements in a growing number of structures, whose medium-long span bridges are surely the most important family. The diffusion of stay cables evidenced, on the other hand, a series of structural troubles, mainly regarding their service behaviour and most of them connected to the uprising of vibrations induced by environmental causes. Such phenomenon is mainly due to the combination of two fundamental characteristics of cables: their very high flexibility and very low inherent damping.
Stay cables dimensions, forces and structural layout can vary a lot in different structures, but the main environmental cause of vibration is doubtless the combined effect of wind and rain (Rain-Wind Induced Vibrations RWIV).

Ph. D. Gabriele Bertagnoli (Author)
DISEG
Politecnico di Torino
Italy

Eng. Dario La Mazza (Co-Author)
DISEG
Politecnico di Torino
Italy

Prof. Eng. Giuseppe Mancini (Co-Author)
DISEG
Politecnico di Torino
Italy

After the first case of RWIV, registered in the '80s [1], many studies of the phenomenon have been done [2] [3] aimed to clarify the causes of the problem and to develop analytical or numerical models able to simulate it. In the same time, several devices able to mitigate RWIV have been developed in order to keep the structures in service in "bad weather" conditions and to reduce or completely avoid the damage induced by RWIV.
Nevertheless, the study of the phenomenon is quite recent and a throughout approach able to describe in a complete way the problem is still under discussion. The main difficulties derive from the big amount of variables entering the problem, mainly related to the structures shape and dimensions and the environmental conditions of the site in which they are built.
The aim of the present study is the analysis of a relevant number of different stay cables without vibration mitigation devices in order to identify which are the main parameters governing the RWIV; a numerical model developed at the University of Aalborg [4] has been calibrated and used for the purpose.

II. Phenomenon Description

A water film is generated by the rain on the external surface of the stay and it is drag by gravity forces towards the bottom part of the stay. The friction between the water film and the wind stream can generally give rise to two water rivulets running along the cable, commonly called upper and lower rivulet, as shown in figure 1.

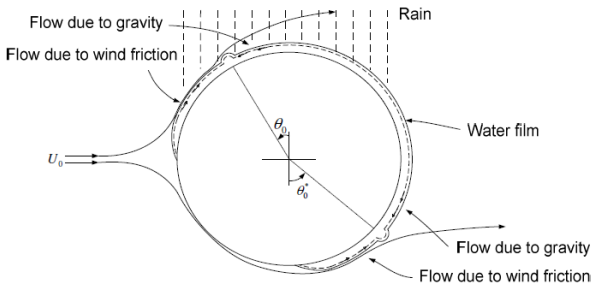

Figure 1. Rivulets formation mechanism.

The angles θ_0 and θ_0^*, which respectively describe the position of the upper and lower rivulets in static equilibrium condition, depend on the wind average speed.
It can be noted that the rivulets can arise in four possible regions, individuated by the angles θ_0 and θ_0^*. In particular, we have two upper regions (upstream, $\theta_0>0$, and downstream, $\theta_0<0$, respect to the wind direction), and two similar lower regions.
It has been demonstrated [5] [6] that the yaw angle β, measured on the horizontal plane between the wind direction and the stay cables' plane (see figure 2a) determines in which of the four regions the two rivulets can be present; moreover, only two rivulets can be contemporary present on the cable.

Both vibrations inside the stay cables plane and outside of it can be contemporary present, and their ratio is again governed by the yaw angle β [5] [6].
The stay cables plane [x,y], the vertical inclination of the stay φ, the average wind speed and direction $\overrightarrow{U_0}$, the component U, in the cables plane and orthogonal to the stay, are presented in figure 2.
When $\beta = 90°$ (wind parallel to the stay cables plane) and the rivulets are oscillating symmetrically with respect to the y direction (figure 2b), only vibrations inside plane [x,y] arise; when $\beta = 0°$ and the rivulets are not oscillating symmetrically with respect to the y direction (figure 2c), only vibrations outside plane [x,y] arise; if $0° < \beta < 90°$ (figure 2d), both vibrations inside and outside plane [xy], arise but the first ones tend to be dominant.

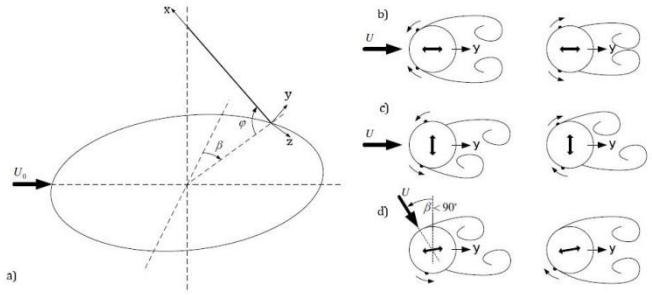

Figure 2. Effect of the yaw angle β (Jensen & Gadegaard, 2009).

Several studies demonstrated both experimentally and numerically that maximum vibration amplitudes are reached when the angle φ, between the stay cable and the horizontal plane, is about 30° and the yaw angle β is about 35° [7] [8] [9]; they also demonstrated that the presence of the rivulet on the upper part of the cables is the main cause of vibration.
Furthermore, Hikami and Shiraishi proposed a range of average wind speed between 9 and 15 m/s in which most of the vibration phenomena take place [1].

III. Model Description

In 2003 Robra [10] proposed a multiple degrees of freedom numerical model shown in figure 3a. In the present work it has been used a simplification of it made by Jensen [4], and shown in figure 3b.

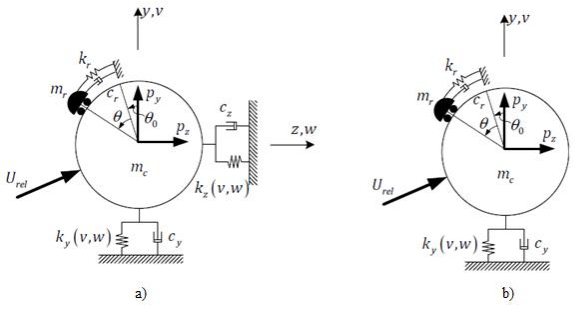

Figure 3. Robra Model and Jensen and Gadegaard simplification.

Jensen and Gadegaard's model neglects the interaction between vibrations inside the stay cables plane [xy] and outside of it. Furthermore, only the upper rivulet in the upstream position is modeled, whereas the influence of the lower rivulet in the downstream position is considered negligible. A non-linear single degree of freedom model, considering only the vibrations of the stay in the [xy] plane, is then chosen for the present work.
This model presents some basic delimitations and assumptions:

- The lift and drag aerodynamics coefficients have been calculated in quasi static flow conditions using a Root Mean Square (RMS) approach.
- Turbulent effects and axial flow effects are neglected.
- Fixed support is considered at both ends of the stay; the displacements of bridge deck and pier or antenna are thus neglected.
- Wind mean speed is assumed constant along the cable although it may change both horizontally and vertically in real conditions.
- Upper rivulet position is assumed to be constant in each finite element in which the cable has been discretized.

All these approximations are commonly accepted in literature, and the authors believe that they can lead to an acceptable degree of accuracy in an engineering study.

The stay has been modelled dividing the chord of the cable into n segments of length L/n. Each finite element is therefore identified by an initial node x_i and a final x_{i+1} as shown in figure 4.

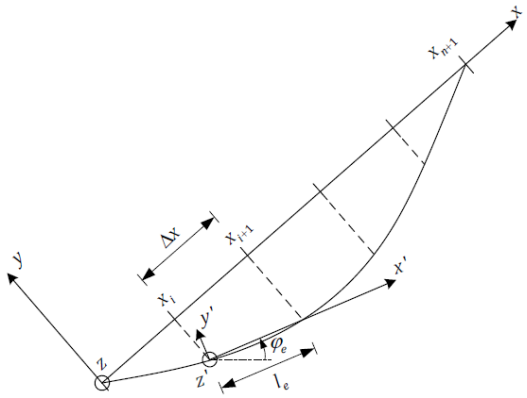

Figure 4. Stay cable model.

Each element has two nodes at the extremities; each node has three displacement (in x, y and z direction) as degrees of freedom (DOF); displacement in the z direction (outside stay cables plane) will be disregarded in this study. The first and the last elements of the stay are fully restrained at the ends (deck and pier connection).
The deflection is assumed to be "small" if compared to the length of the stay, so the prestressing force is considered constant along the cable.
The following formulation is based on the theory proposed by Nielsen [11].
The initial deformed shape of the stay is assumed to be parabolic following equation (1):

$$y(x) = -4f\left(1 - \frac{x}{L}\right)\frac{x}{L} \qquad (1)$$

Where deflection f is given by:

$$f = \frac{1}{8}\frac{\mu g L^2}{F_0}\cos\varphi \quad (2)$$

where: μ is the mass per unit length of the stay, g is gravity acceleration, L is the length of the stay, F_0 is the prestressing force and φ is the stay cable inclination respect to the horizontal plane (see figure 2a).
The length l_e and the inclination φ_e (respect to the horizontal plane) of each element are defined in function of the angle between the local axis x' and the global one x.
Figure 5 shows a single element in its deformed shape. The dynamic displacement vector in the local referring system [x',y', z'] is called $v_e'(x',t)$ and has the following components along the local axes: $v_x'(x',t)$, $v_y'(x',t)$ and $v_z'(x',t)$.
In the same way, the dynamic external load per unit length vector, $p_e'(x',t)$ has the following components along the local axes: $p_x'(x',t)$, $p_y'(x',t)$ and $p_z'(x',t)$.
The six degrees of freedom in the local system [x',y'] are assembled in the vector $q_e'^T(t) = [q_1'(t), \ldots, q_6'(t)]$, where $q_1'(t), \ldots, q_6'(t)$ are the components of the displacements of the extremities of the element in the local referring system [x',y', z']. The vector of the nodal loads corresponding to q_e' is called $r_e'(t) = [r_1'(t), \ldots, r_6'(t)]$.

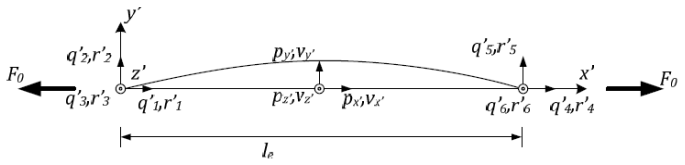

Figure 5. Element definition in the local referring system.

The displacements inside each element $v_e'(x',t)$, in the local referring system, are approximated using linear interpolation between nodal values as follows:

$$v_e'(x',t) = N(x')q_e'(t) \quad (3)$$

The matrix of the shape functions N(x') is:

$$N(x') = \begin{bmatrix} N_1(x') & 0 & 0 & N_2(x') & 0 & 0 \\ 0 & N_1(x') & 0 & 0 & N_2(x') & 0 \\ 0 & 0 & N_1(x') & 0 & 0 & N_2(x') \end{bmatrix} \quad (4)$$

where:

$$N_1(x') = 1 - \frac{x'}{l_e} \quad , \quad N_2(x') = \frac{x'}{l_e} \quad (5)$$

The cinematic equation in the local referring system is written by means of Lagrangian equation:

$$L_e(q_e', q_e') = T_e(q_e') - U_e(q_e') \quad (6)$$

where the kinetic energy $T_e(q_e')$ and potential energy $U_e(q_e')$, including the potential energy of the conservative external loads and reaction forces, are given as:

$$T_e(q_e') = \int_0^{l_e} \frac{1}{2}\mu\left(\left(\frac{\partial v_x'}{\partial t}\right)^2 + \left(\frac{\partial v_y'}{\partial t}\right)^2 + \left(\frac{\partial v_z'}{\partial t}\right)^2\right)dx' = \frac{1}{2}q_e'^T(t)M_e'q_e'(t) \quad (7)$$

$$U_e(q_e') = \int_0^{l_e}\frac{1}{2}AE\left(\left(\frac{\partial v_x'}{\partial x'}\right)^2 + \left(\frac{\partial v_y'}{\partial x'}\right)^2 + \left(\frac{\partial v_z'}{\partial x'}\right)^2\right)dx' - \int_0^{l_e}\left(p_{x'}v_{x'} + p_{y'}v_{y'} + p_{z'}v_{z'}\right)dx' = \frac{1}{2}q_e'^T(t)K_e'q_e'(t) - q_e'^T(t)p_e'(t) - q_e'^T(t)r_e'(t) \quad (8)$$

The consistent mass matrix $[M_e']$, the stiffness matrix $[K_e']$ and nodal load vector $[p_e']$ are given as:

$$M_e' = \int_0^{l_e}\mu N_e^T(x')N_e(t)dx' \frac{\mu l_e}{6}\begin{bmatrix} 2 & 0 & 0 & 1 & 0 & 0 \\ 0 & 2 & 0 & 0 & 1 & 0 \\ 0 & 0 & 2 & 0 & 0 & 1 \\ 1 & 0 & 0 & 2 & 0 & 0 \\ 0 & 1 & 0 & 0 & 2 & 0 \\ 0 & 0 & 1 & 0 & 0 & 2 \end{bmatrix} \quad (9)$$

$$K_e' = \frac{1}{l_e}\begin{bmatrix} AE & 0 & 0 & -AE & 0 & 0 \\ 0 & F_0 & 0 & 0 & -F_0 & 0 \\ 0 & 0 & F_0 & 0 & 0 & -F_0 \\ -AE & 0 & 0 & AE & 0 & 0 \\ 0 & -F_0 & 0 & 0 & F_0 & 0 \\ 0 & 0 & -F_0 & 0 & 0 & F_0 \end{bmatrix} \quad (10)$$

$$p_e'(t) = \int_0^{l_e} N^T(x')\,p_e'(x',t)dx' = \begin{bmatrix} \int_0^{l_e} N_1(x')p_x'(x',t)dx' \\ \int_0^{l_e} N_1(x')p_y'(x',t)dx' \\ \int_0^{l_e} N_1(x')p_z'(x',t)dx' \\ \int_0^{l_e} N_2(x')p_x'(x',t)dx' \\ \int_0^{l_e} N_2(x')p_y'(x',t)dx' \\ \int_0^{l_e} N_2(x')p_z'(x',t)dx' \end{bmatrix} = \frac{l}{2}\begin{bmatrix} p_x'(t) \\ p_y'(t) \\ p_z'(t) \\ p_x'(t) \\ p_y'(t) \\ p_z'(t) \end{bmatrix} \quad (11)$$

In the final result of (11) it has been assumed that the loads per unit length are constant within the element length. The Lagrange equations of the motion of one element can then be written as:

$$\frac{d}{dt}\left(\frac{\partial l_e}{\partial \dot{q}_e^T}\right) - \frac{\partial l_e}{\partial q_e^T} = -C_e'q_e' \rightarrow M_e'\ddot{q}_e' + C_e'\dot{q}_e' + K_e'q_e' = p_e'(t) + r_e'(t) \quad (12)$$

where C_e' is the linear viscous element damping matrix. The damping matrix is assumed to be proportional to the mass and stiffness matrices according to Rayleigh damping model.

$$C_e' = a_0M_e' + a_1K_e' \quad (13)$$

The two damping coefficients α_0 and α_1 are determined from the corresponding global structural damping matrix as indicated in the following paragraph.

IV. Stay's Cinematic Equations

The cinematic equation of one element in the global coordinate system (X,Y,Z) reads:

$$M_e\ddot{q}_e + C_e\dot{q}_e + K_eq_e = p_e(t) + r_e(t)_e' \quad (14)$$

The transformation between local and global components of the nodal displacements may be written as:

$$q_e(t) = A_e q'_e(t) \quad (15)$$

The corresponding transformation between local and global components of the element mass (M_e), damping (C_e) and stiffness matrices (K_e), external loads (p_e) and reaction vectors (r_e) read

$$M_e = A_e^T M'_e A_e \quad , \quad C_e = A_e^T C'_e A_e \quad , \quad K_e = A_e^T K'_e A_e \quad , \quad p_e(t) = A_e^T p'_e(t) \quad , \quad r_e(t) = A_e^T r'_e(t) \quad (16)$$

Where matrix A_e is:

$$A_e = \begin{bmatrix} A_{0e} & 0 \\ 0 & A_{0e} \end{bmatrix} \quad , \quad A_{0e} = \begin{bmatrix} cos\varphi_e & -sin\varphi_e & 0 \\ sin\varphi_e & cos\varphi_e & 0 \\ 0 & 0 & 1 \end{bmatrix} \quad (17)$$

And the angle φ_e is given in figure 4.
The global equation of motion is found by substitution of equations (15) and (16) into equation (14) and correction for kinematic boundary conditions:

$$M_s \ddot{v}_s + C_s \dot{v}_s + K_s v_s = p_s(\theta_s, \dot{v}_s) \quad (18)$$

Where $v_s = v_s(t), \dot{v}_s = \dot{v}_s(t)$ e $\ddot{v}_s = \ddot{v}_s(t)$ are respectively the time dependent displacement, velocity, and acceleration vector in the global coordinate system (X,Y,Z) whereas M_S, C_S e K_S are the structural mass, damping, and stiffness matrices. According to (13) α_0 and α_1 are calculated in order to represent with the damping matrix the 1st and 2nd in-plane modal damping ratios related to the first and second eigenmode of the stay ζ_1 and ζ_2. This procedure needs a calibration as explained by Nielsen [11].

$$\begin{bmatrix} a_0 \\ a_1 \end{bmatrix} = \frac{2\omega_1\omega_2}{\omega_2^2 - \omega_1^2} \begin{bmatrix} \omega_2 & -\omega_1 \\ -\frac{1}{\omega_2} & \frac{1}{\omega_1} \end{bmatrix} \begin{bmatrix} \zeta_1 \\ \zeta_2 \end{bmatrix} \quad (19)$$

where ω_1 and ω_2 are the undamped angular frequencies of the two lowest in-plane eigenmodes, and ζ_1 and ζ_2 are the corresponding modal damping ratios, which are assumed to be known.
Only loads in the y' direction (inside stay cable plane) are considered, whereas out-of-plane loads are neglected. The load per unit length may be expressed as follows:

$$p_{y',e}(\theta_e, v_{y',e}) = p_{y',0} + p_{y',1} v_{y',e} + p_{y',2} \theta_e \quad (20)$$

where $\theta_e = \theta_e(t)$ is the angle describing the dynamic position of the rivulet which is assumed constant along each finite element (see figure 3). The three components at the second member of (20) represent the quasi-static contribution, the aerodynamic viscous damping term, and an aerodynamic stiffness term, respectively. Equation (20) can be written in matrix form and expressed in global coordinates as follows:

$$\underset{mx1}{p_s(\theta_s, \dot{v}_s)} = \underset{mxn\ nx1}{K_1 \theta_s} + \underset{mxm\ mx1}{C_1 \dot{v}_s} + \underset{mx1}{p_0} \quad (21)$$

where:

$$\theta_s(t) = \begin{bmatrix} \theta_1(t) \\ \vdots \\ \theta_n(t) \end{bmatrix} \quad , \quad v_s(t) = \begin{bmatrix} v_1(t) \\ \vdots \\ v_m(t) \end{bmatrix} \quad (22)$$

$$K_1 = -\frac{1}{2} \begin{bmatrix} k_1 & k_2 & 0 & 0 & 0 \\ 0 & k_2 & k_3 & \ddots & \vdots \\ 0 & 0 & k_3 & \ddots & 0 \\ 0 & \ddots & \ddots & \ddots & 0 \\ 0 & \dots & 0 & 0 & k_n \end{bmatrix} \quad , \quad k_i = l_{e,i} p_{y',2} \begin{bmatrix} -sin\varphi_i \\ cos\varphi_i \\ 0 \end{bmatrix} \quad (23)$$

$$C_1 = \frac{1}{4} \begin{bmatrix} c_1 & c_2 & 0 & 0 & 0 \\ 0 & c_2 & c_3 & \ddots & \vdots \\ 0 & 0 & c_3 & \ddots & 0 \\ 0 & \ddots & \ddots & \ddots & 0 \\ 0 & \dots & 0 & 0 & c_n \end{bmatrix},$$

$$c_i = l_{e,i} p_{y',1} \begin{bmatrix} sin^2\varphi_i & -sin\varphi_i cos\varphi_i & 0 \\ -sin\varphi_i cos\varphi_i & cos^2\varphi_i & 0 \\ 0 & 0 & 0 \end{bmatrix} \quad (24)$$

$$p_0 = \frac{1}{2} \begin{bmatrix} p_{0,1} \\ p_{0,2} + p_{0,1} \\ \vdots \\ p_{0,m-1} + p_{0,m-2} \\ p_{0,m} \end{bmatrix} \quad , \quad p_{0,i} = l_{e,i} p_{y',0} \begin{bmatrix} -sin\varphi_i \\ cos\varphi_i \\ 0 \end{bmatrix} \quad (25)$$

v. Calibraton Procedure

The finite element code proposed by Jensen has been tested on three bridges, used as benchmark cases, whose data concerning RWIV where completely known in literature: Meiko Nishi Bridge (built in Nagoya in 1985), Erasmus Bridge (built in Rotterdam in 1996) and Pont de Normandie (built in Le Havre-Honfleur in 1995).
The data used in the calibration of the model for each bridge are resumed in Table 1.

TABLE 1. CALIBRATION DATA

	Meiko Nishi	*Erasmus*	*Normandie*
Stay length	75 m	300 m	440 m
Stay diameter	140 mm	225 mm	300 mm
Number of strands per stay	19	42	102
Strand cross section	150 mm2	150 mm2	150 mm2
Stay self-weight	51 kg/m	70 kg/m	133 kg/m
Steel elastic modulus	195 GPa	195 GPa	190 GPa
Stress in serviceability conditions	400 MPa	650 MPa	650 MPa
Dischinger modulus	187 GPa	184 GPa	176 GPa
Vertical angle between stay and deck	45 °	22 °	17.5 °
Inherent damping	0.11 %	0.18 %	0.10 %
Maximum vibration amplitude	550 mm	1400 mm	1500 mm
Average wind speed	10 m/s	14 m/s	12 m/s
Wind yaw angle	45 °	25 °	35 °

- Meiko Nishi Bridge

The Meiko Nishi West Bridge has been the first one to undergo RWIV [1] [12]. Vibrations reached a maximum asymptotic value of about 550m after about 15 minutes. These values were found in the numerical simulation using an inherent damping factor of 0.18%, that is 1.6 times the value given by the authors [12]. This difference can be explained by the fact that during RWIV the cable is subjected to displacements that are bigger than the ones used to measure the inherent damping, and it is thus able to dissipate a bigger amount of energy than the foreseen one.

The oscillation of the upper rivulet increases in time and stabilizes itself after about ten minutes within the interval $-15° \leq \theta \leq +10°$.

- Erasmus Bridge

Few months after the opening of the bridge, very big vibrations of the cables were registered, accompanied by deck oscillation that requested the temporary closure of the bridge [13].
Stay cable vibrations reached an asymptotic value of 1400mm after about 5 minutes of wind action. These values were found in the numerical simulation using an inherent damping factor of 0.72%, that is 4 times the value given by Geurts [13]. As for the Meiko Nishi Bridge, this difference can be explained with the amplitude of the vibrations.
The oscillation of the upper rivulet increases in time and stabilizes itself after about three minutes within the interval $-15° \leq \theta \leq +15°$.

- Pont de Normandie

When it was opened, the Pont de Normandie was the biggest stay cable bridge ever built (850m).
Immediately after the bridge opening, big amplitude vibrations of the stays were registered during rainstorms of moderate intensity [14].
Stay cable vibrations reached an asymptotic value of 1500mm after about 5 minutes of wind action. These values were found in the numerical simulation using an inherent damping factor of 0.75%, that is 7.5 times the value given by Flamand [14]. The same explanation given in the previous cases can be applicable also to this case.
The oscillation of the upper rivulet increases in time and stabilizes itself after about ten minutes within the interval $-17° \leq \theta \leq +15°$.

VI. Parametric Analisys Input Data

After the calibration procedure described in the previous paragraph, a parametric study has been done in order to investigate which are the main factors that can control RWIV.
Seven different parameters have been identified: wind speed, length of the stay, diameter of the stay (in function of the number of strands of it), stay cable inclination with respect to the horizontal plane, ratio between the force present in the stay in service conditions and the ultimate strength of it, inherent damping, and wind yaw angle. Two values have been chosen for each parameter apart from the stay length, which was represented by three different values, reaching a total of 432 different cases. The values chosen are listed in the following, and fall within the range considered potentially dangerous for RWIV by literature:

1. Average wind speed U: 10m/s – 15m/s.
2. Stay cable length ls: 100m – 200m – 300m.
3. Number of strands of the stay cable ns: 31 – 61.
4. Stay cable inclination with respect to horizontal plane φ: 20° - 30° - 40°.
5. Ratio between service and ultimate force in the stay P/Pu: 35% - 45%.
6. Inherent damping c: 0,18% - 0,72%.
7. Wind yaw angle (see figure 2a) β: 15° - 25° - 40°.

The wind action has been applied for each case for five minutes time, being this period long enough to check the sensitivity to RWIV of each stay.

VII. Parametric Analysis Results

The results of the 432 analyses can be grouped into six different families according to the stay behaviour, as presented hereafter:

1. The stay does not vibrate, or, being more precise, small initial vibrations of few centimeters occur, but they immediately decrease after a few seconds. The position of the upper rivulet is constant in time.
2. The stay vibrates with a moderate amplitude and reaches a stabilized oscillation before the end of the investigation period of 300s. The upper rivulet oscillation is also stable and covers a few degrees around its static equilibrium position.
3. The stay vibrates with small amplitude but after 300s it has not reached an asymptotic condition, that is the vibration is small but still increasing with no sign of stabilization.
4. The stay undergoes big amplitude vibrations, but find an asymptotic condition in which vibrations are not increasing any more within the 300s interval. In the most unfavorable cases the vibration amplitude can reach 1/50 of the stay length. The upper rivulet is also subjected to big amplitude oscillations.
5. The stay undergoes big amplitude vibrations but does not find an asymptotic condition within the 300s interval. In the most unfavorable cases, the vibration amplitude can reach 1/80 of the stay length and it is still growing after 300s. The upper rivulet is also subjected to growing amplitude oscillations.
6. Some geometrical configurations avoid completely the birth of the RWIV phenomenon: if the stay inclination respect to the horizontal plane is 40°, the wind speed is 15m/s, and the yaw angle is 40°, non vibrations can arise regardless of the other variables, because the position of the upper rivulet does not interfere with the aerodynamic configuration of the stay.

The occurrences for each of the six families described above and an example of each behaviour are resumed in Table 2.

TABLE 2. PARAMETRIC ANALYSIS RESULTS

Family		***1***	***2***	***3***	***4***	***5***	***6***
Vibration amplitude/Stay length	-	$\frac{a}{l_s} < \frac{1}{2000}$	$\frac{1}{2000} < \frac{a}{l_s} < \frac{1}{500}$		$\frac{a}{l_s} > \frac{1}{500}$		0
Number of occurrences	-	306	14	9	18	34	51
Percentage ratio of occurrences	%	70.8	3.2	2.1	4.2	7.9	11.8
Examples							
Average wind speed	m/s	15	15	10	15	15	15
Inherent damping	%	0.18	0.72	0.18	0.72	0.18	any
Stay axial load ratio	%	35	35	45	35	35	any
Number of strands	-	31	31	61	31	31	any
Stay length	m	300	200	200	300	300	any
Stay inclination	°	20	20	40	20	40	40
Wind yaw angle	°	40	15	40	15	15	40
First natural frequency	Hz	2.56	3.83	4.15	2.56	2.90	any

VIII. Results Discussion

After the individuation of the main behaviors of the stays, the effect of each of the seven parameters presented before on the sensitivity of the stays to RWIV has been studied. For each parameter the results have been grouped into two big classes: "vibrating stays" (family 2, 3, 4 and 5) and "not vibrating stays" (family 1 and 6).

The first parameter investigated is the wind average speed, which plays an important role: passing from 10 m/s to 15 m/s the number of stays subjected to vibrations increases and almost triples, passing from 8.8% to 25.9% of the total as shown in figure 6.

The second parameter investigated is the stay cable length, which again plays an important role (figure 7). Three different lengths have been studied: short (100m), medium (200m), long (300m); the number of stays subjected to vibrations is nil for the first length, 20.1% for the second and 31.9% for the long ones.

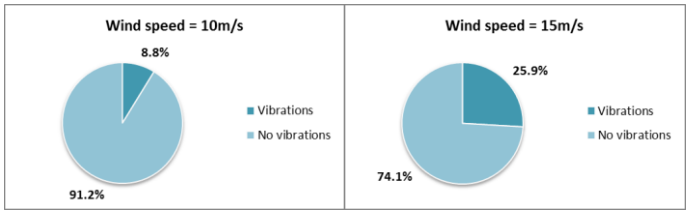

Figure 6. Effect of wind speed

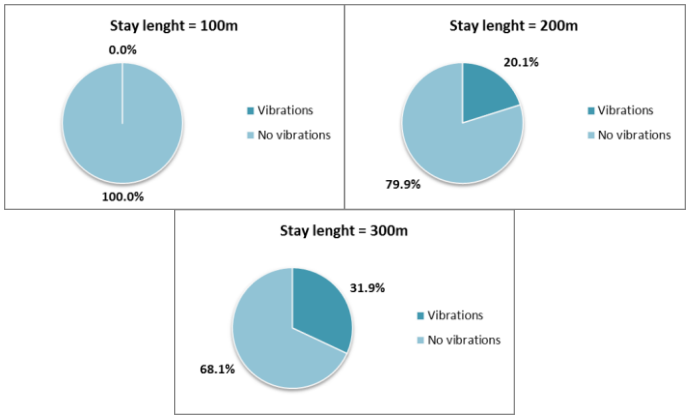

Figure 7. Effect of stay length

RWIV seems then to affect only stays longer than 100m, and the longer the stay is the bigger is the risk to undergo RWIV.

The third parameter investigated is the stay diameter, which is related to the number of strands. Two different diameters have been chosen: a small one (16cm, corresponding to 31 strands) and a big one, (25cm, corresponding to 61 strands). This parameter seems to have no effect on the sensitivity of the stay to the RWIV: 19% of the small diameter stays and 15.7% of the big diameter stays vibrates (figure 8).

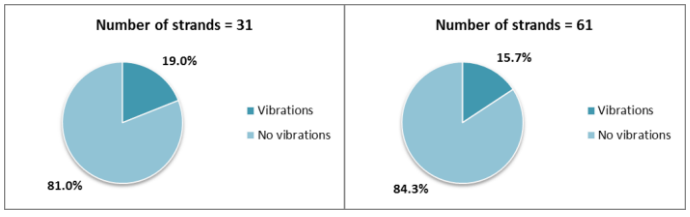

Figure 8. Effect of number of strands (stay diameter)

The fourth parameter investigated is the stay cable inclination, φ, with respect to the horizontal plane. Three different configurations have been tested: small (20°), medium (30°) and big (40°) that may represent a bridge antenna tall about 18%, 29% and 42% of the central span. The results are shown in figure 9. This parameter seems to have little effect as the number of vibrating stays varies between 18.8% and 16% for the three configurations.

The fifth parameter investigated is the axial load ratio, that is the force stressing the stay due to deck weight and prestressing. The values chosen are respectively 35% and 45% of the load that will break the stay.

These values are commonly found in service conditions in stay cables. This parameter seems to have no effect on the sensitivity of the stay to the RWIV: the amount of vibrating stays with axial load ratio equal to 35% is 18.1%, whereas it becomes 16.7% for an axial load ratio of 45% (figure 10).

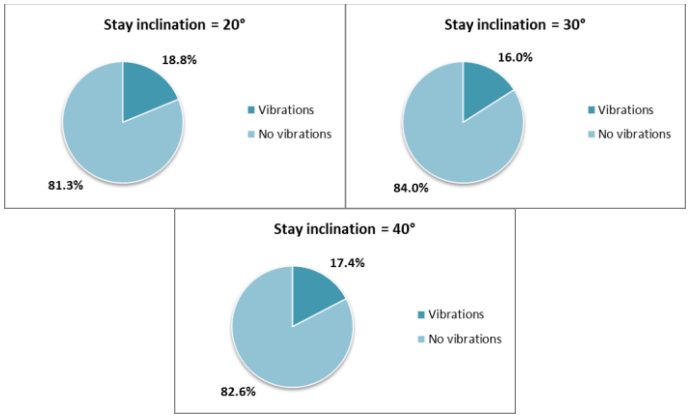

Figure 9. Effect of stay inclination on the horizontal plane

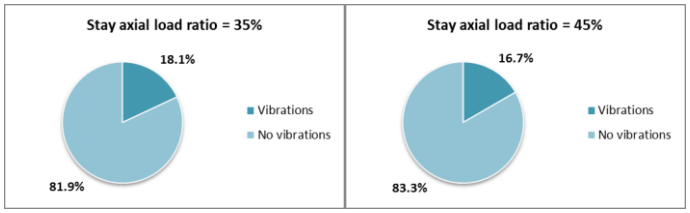

Figure 10. Effect of axial load ratio

The sixth parameter taken into account is the inherent damping. This factor plays an important role, and it is not easy to carefully measure it. Damping is, in fact, function of the magnitude of the vibration: small amplitude vibrations can activate small values of inherent damping, whereas big amplitude ones activate higher values of damping. As tests on real scale stays are very difficult to be realized forcing big amplitude vibrations, it is authors' opinion that inherent damping can be easily underestimated. Values of inherent damping found in literature for stays are generally variables between 0.1% and 0.2%, but the calibration procedure proposed in the present paper has suggested that sometimes inherent damping can reach values close to 1%.

A higher damping factor limits of course the magnitude of vibrations, but reduces also the number of stays that are affected by RWIV: 21% of the total number of stays with

c=0.18% vibrates, whereas only 13.4 of the total number of stays with c=0.72% undergoes RWIV (figure 11).

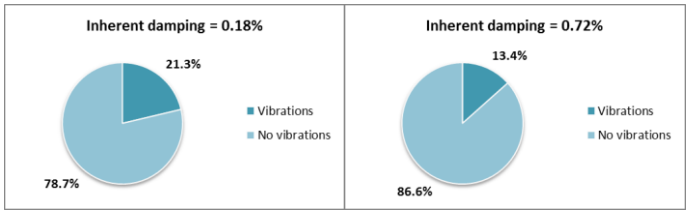

Figure 11. Effect of inherent damping

The seventh and last parameter investigated is the wind yaw angle: three different values of 15° (wind almost orthogonal to the bridge axis and therefore to the stay cable plane), 25° and 40° (wind impacting the bridge in skew direction) have been tested. The results are presented in figure 12.

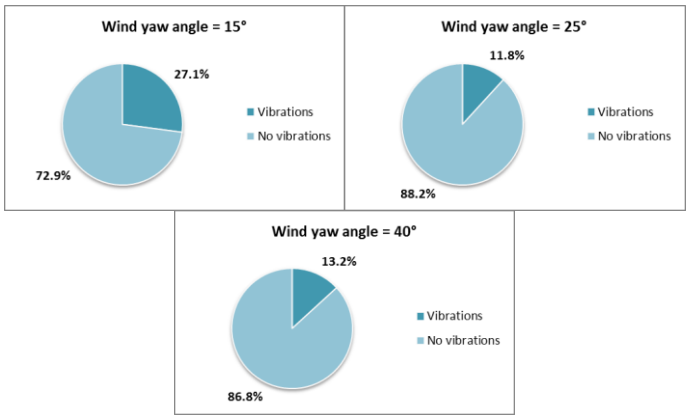

Figure 12. Effect of yaw angle

It can be noticed that if the wind is almost orthogonal to the stay cables plane the number of vibrating stays is quite high (about 27%), whereas it decreases to almost one half (13.5%) if the wind becomes quite skew with respect to the cable stay plane.

This result can be read in combination with the considerations done on the wind speed: the 27.1% of stays that vibrates with the yaw angle of 15° is mostly the same 25.9% associated with the wind speed of 15 m/s; in the same way, the 13.2% of stays that vibrates with the wind yaw angle of 40° is associated with the wind speed of 10 m/s. The wind component in the plane of the stays that generates vibrations can be achieved with high total speed and small yaw angle or low total speed and big yaw angle.

A perfect correlation cannot be seen as three different yaw angles have been taken into account but only two wind speeds. The authors believe that adding in the parametric study a third wind speed, of about 12.5 m/s, could lead to a stricter correlation between yaw angles and wind speeds, mostly changing the results relative to 25° yaw angle.

When the angle of attack between the wind direction and the position of the upper rivulet becomes too big, the upper rivulet does not interfere any more with the cable aerodynamics moving on the upper downstream position. When, on the contrary, the attack angle results to be too small, the upper rivulet can move towards the bottom of the cable dragged by gravity force, and again it stops to interfere with the cable aerodynamics.

IX. Conclusions

The aim of the present work was to calibrate a numerical finite element model developed at Aalborg University [4] on real life cases where vibration data were completely available.

The calibration show the importance of the correct evaluation of the inherent damping of the stay cables; values usually proposed in literature (between 0.1% and 0.2%) can underestimate the real damping capacity of the stays, and lead to an incorrect prediction of the vibration sensitivity and/or amplitude. Values of inherent damping up to 0.7÷0.8% have led to good agreement between numerical predictions and measured data.

After the calibration the model has been used to run a parametric study of the factors influencing RWIV in stay cables without vibration controls systems such as ducts with helical fillets, tying ropes or passive, semi-active or active controls.

Seven different parameters have been taken into account: stay cable length, diameter, force, angle of inclination on the horizontal, inherent damping, wind speed and yaw angle.

Some parameters have demonstrated to lead the response in a sensible way, whereas some others seem not to influence the phenomenon.

In particular, the stay cable length has a big influence as longer cables are more easily affected by RWIV, whereas cables under 100m length seems to be never interested by the problem. Stay cable inclination, wind speed and wind yaw angle have also a significant role, and especially wind speed and wind yaw angle seem to be strictly connected.

On the contrary, the axial load ratio and the diameter of the stay have almost no influence on the response.

As a conclusion the number of stays that presented sensitivity to RWIV is quite small (17.4%) compared to the total number of simulations performed in the study.

The parametric analysis is now under refinement testing a wider range of values for each of the parameters presented, and it will be object of future publication. Some simple indications that will allow the designer to understand the risk of RWIV for a given bridge without performing complicated non-linear dynamic analyses could be derived in next future from these results.

X. References

[1] Y. Hikami and N. Shiraishi, "Rain/wind-induced vibrations of Cable in Cable-Stayed Bridges", Journal of Wind Engineering and Industrial Aerodynamics, vol. 29, pp. 409-418, 1988

[2] U. S. FHWA, Department of Transportation, Wind-Induced Vibration of Stay Cables, Research, Development, and Technology Turner-Fairbank Highway Research Center, 2007

[3] E. De Sà Caetano, Cable Vibrations in Cable-Stayed Bridges, IABSE-AIPC-IVBH, Zurich, 2007, ISBN 978-3-85748-115-4

[4] J. Jensen and C. Gadegaard, Rain/wind induced vibrations of stay-cables, Master Thesis, Aalborg University, Department of Civil Engineering, Aalborg, 2009

[5] C. Verwiebe, "Neue Erikenntnisse uber die Erregermechanismen Regen-Wind-induierter Scwingungen", Stahlbau, vol. 65, pp. 547-550, 1996

[6] C. Verwiebe, "Rain-wind-induced vibrations of cables and bars" in A. Larsen and S. Esdahl, (eds), Bridge Aerodynamics, Balkema, 1998, pp. 255-263
[7] Y. Hikami, "Rain vibrations of cables of cable-stayed bridges", Journal of Japan Association of Wind Engineering, vol. 27, pp. 17-28, 1986
[8] M. Gu and X. Du, "Experimental investigation of rain-wind induced vibration of cables in cable-stayed bridges and its mitigation", Journal of wind engineering and industrial aerodynamics, vol. 93, pp. 79-95, 2004
[9] M. Gu, X. Du and S. Y. Li, "Experimental and theoretical simulations on wind-rain induced vibrations of 3-D rigid stay cables", Journal of Sound and Vibration, vol. 320, n. 1-2, pp. 184-200, 2008
[10] J. Robra, Regen-Wind-induzierte Schwingungen von Schragkabeln und Hangern - Ein Rechenmodell zur Vorhersage und Massnahmen zur Verhinderung, Dissertation Technische Universitat Wien, Austria, 350p., 2003
[11] S. R. K. Nielsen, Vibration Theory, vol. 1 Linear Vibration Theory, Aalborg: Aalborg tekniske Universitetsforlag, 2004, ISSN: 1395-8232 U2004-1
[12] H. J. Zhou and Y. L. Xu, "Wind–rain-induced vibration and control of stay cables in a cable-stayed bridge" Structural Control and Health Monitoring, vol. 14, n. 7, pp. 1013-1033, 2007
[13] C. Geurts, T.Vrouenwelder, P. Staalduinen and J. Reusink, "Numerical Modelling of Rain-Wind-Induced Vibration: Erasmus Bridge, Rotterdam", Structural Engineering International, vol. 8, n. 2, pp. 129-135, 1998
[14] O. Flamand, "Rain-wind induced vibration of cables", Proceedings of 1st IAWE European and African Regional Conference, Guernsey, 1993